Imaginary gap-closed points and dynamics in a class of dissipative systems

Shicheng Ma [1,*] Heng Lin [2,*,†] and Jinghui Pi [2,‡]
[1]*School of Physics, Nankai University, Tianjin 300071, China*
[2]*Department of Physics, Tsinghua University, Beijing 100084, China*

(Received 12 March 2024; revised 22 May 2024; accepted 14 June 2024; published 24 June 2024)

We investigate imaginary gap-closed (IGC) points and their associated dynamics in dissipative systems. In a general non-Hermitian model, we derive the equation governing the IGC points of the energy spectrum, establishing that these points are only determined by the Hermitian part of the Hamiltonian. Focusing on a class of one-dimensional dissipative chains, we explore quantum walks across different scenarios and various parameters, showing that IGC points induce a power-law decay scaling in bulk loss probability and trigger a boundary phenomenon referred to as "edge burst." This observation underscores the crucial role of IGC points under periodic boundary conditions (PBCs) in shaping quantum walk dynamics. Finally, we demonstrate that the damping matrices of these dissipative chains under PBCs possess Liouvillian gapless points, implying an algebraic convergence towards the steady state in long-time dynamics.

DOI: 10.1103/PhysRevB.109.214311

I. INTRODUCTION

The field of non-Hermitian physics has witnessed remarkable development over the past few decades [1–6]. In classical systems, non-Hermiticity is introduced through controlled gain or loss and leads to novel phenomena beyond Hermitian counterparts [7–20]. In quantum systems, effective non-Hermitian Hamiltonians arise from conditional dynamics under continuous monitoring and postselection of null measurements [21–26] or via the Feshbach projection formalism [27–30]. Realizations of non-Hermitian systems span diverse open quantum platforms [31–41]. Notably, non-Hermitian Hamiltonians can exhibit peculiar properties, for instance, the existence of exceptional points [42–46], which induce novel universality classes of phase transitions in non-Hermitian quantum systems [47–60]. Another unique feature of non-Hermitian systems is the non-Hermitian skin effect (NHSE), namely, the anomalous localization of an extensive number of bulk-band eigenstates at the edges [61–64]. The NHSE plays a central role in the non-Hermitian topological phases and reshapes convectional bulk-boundary correspondence [65–90]. The topology origin of the NHSE is intimately linked to the point gap of non-Hermitian Bloch Hamiltonians [91,92].

On the other hand, the NHSE also induces novel dynamical phenomena in open quantum systems. These include damping behavior and diverging relaxation time in Liouvillian dynamics [93–97], directional amplification of signals [98,99], self-healing of skin modes [100], and directional invisibility of scattered wave packet [101,102]. Intriguingly, non-Hermitian dynamics exhibit boundary condition independence in the thermodynamic limit [103]. However, in finite-size systems, energy spectra under open boundary conditions (OBCs) show dramatic differences from those under periodic boundary conditions (PBCs) due to the NHSE [62,90,91]. Thus, one may question which non-Hermitian Hamiltonians determine the dynamical evolution of the systems. Furthermore, the boundary's role is also crucial to understanding non-Hermitian dynamics.

Motivated by the above questions, we first analyze a general non-Hermitian model whose non-Hermiticity comes from the onsite dissipation. Our investigation centers on imaginary gap-closed (IGC) points, which are eigenstates possessing real energies and dictate the long-time behavior of the system [104]. Notably, these IGC points depend solely on the Hermitian component of the Hamiltonian, unaffected by dissipative terms. Furthermore, IGC states are populated on nondissipative sites and can be viewed as dark modes. When focusing on a class of one-dimensional dissipative models, the PBC spectra exhibit IGC points, while their OBC counterparts lack such points as eigenstates feature the NHSE. By introducing the non-Hermitian quantum walk, we investigate the relation between IGC points and the scaling behavior of bulk loss probability in space. Consequently, these IGC points lead to a spatial power-law decay of the loss probability in the bulk of the system. Moreover, an associated boundary phenomenon, termed "edge burst," emerges. Specifically, when a quantum particle is initially prepared on a specific bulk site, there is a prominent peak in the loss probability at the edge. We discuss this phenomenon in different quantum walk scenarios and the impact of various parameters, showing the universality of the correlation between edge burst and IGC points. Finally, we analyze the Liouvillian dynamics and demonstrate that damping matrices of these dissipative chains under PBCs can have Liouvillian gapless points, implying an algebraic convergence towards the steady state in long-time dynamics.

*These authors contributed equally to this work.
†Contact author: linh1721@outlook.com
‡Contact author: pijh14@gmail.com

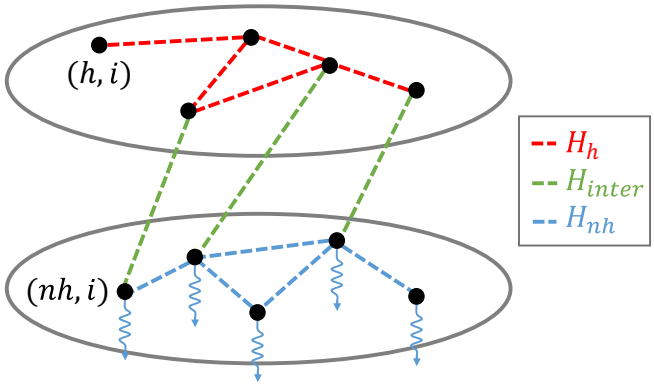

FIG. 1. The general non-Hermitian lattice model. Red: interactions within nondissipative sites; blue: interactions within dissipative sites; green: interactions between nondissipative sites and dissipative sites.

This paper is organized as follows. In Sec. II, we introduce a general non-Hermitian model and analyze its IGC points. In Sec. III, we investigate the quantum walk dynamics in a class of one-dimensional dissipative chains. In Sec. IV, we discuss the impact of various parameters on quantum walks. In Sec. V, we demonstrate that IGC points of the PBC Liouvillian spectrum capture the long-time dynamics of the system. Finally, a summary is given in Sec. VI.

II. NON-HERMITIAN MODEL AND UNIVERSAL IMAGINARY GAPLESS MODES

Let us first consider a general non-Hermitian lattice model (Fig. 1), whose non-Hermiticity totally comes from the onsite dissipation. We classify the lattice sites into two categories: nondissipative sites and dissipative sites, denoted by (h, i) and (nh, i), respectively. Then, the Hamiltonian of this system can be divided into three parts,

$$H = H_h + H_{nh} + H_{\text{inter}}, \tag{1}$$

where H_h is the interaction within nondissipative sites, H_{nh} is the interaction within dissipative sites, and H_{inter} is the interaction between nondissipative sites and dissipative sites. Their expressions are given by

$$\begin{aligned} H_h &= \sum_{i,j} a_{ij} \left|h, i\right\rangle \left\langle h, j\right|, \\ H_{nh} &= \sum_{i,j} b_{ij} \left|nh, i\right\rangle \left\langle nh, j\right|, \\ H_{\text{inter}} &= \sum_{i,j} (c_{ij} \left|nh, i\right\rangle \left\langle h, j\right| + \text{H.c.}), \end{aligned} \tag{2}$$

where coefficients a_{ij}, b_{ij}, and c_{ij} are complex numbers, satisfying $a_{ij} = a_{ji}^*$, $b_{ij} = b_{ji}^* (i \neq j)$, and $\text{Im}(b_{ii}) < 0$ for all i and j. Thus, H_h and H_{inter} are Hermitian operators, while H_{nh} is non-Hermitian.

The imaginary part of the system's energy spectrum must be smaller than or equal to zero for its dissipative nature. Now we assume the existence of IGC points in the energy spectrum, i.e.,

$$\begin{aligned} &\exists \left|\text{IGC}\right\rangle, \quad \text{so that } H \left|\text{IGC}\right\rangle = E_{\text{IGC}} \left|\text{IGC}\right\rangle, \\ &\text{and } \text{Im}(E_{\text{IGC}}) = 0. \end{aligned} \tag{3}$$

Subsequently, we discuss the conditions these IGC states should satisfy. Begin with the Lemma 1.

Lemma 1. In systems where non-Hermiticity arises solely from onsite dissipation [Eq. (2)], the wave functions of IGC states are only populated on nondissipative sites, i.e.,

$$\left|\text{IGC}\right\rangle = \sum_i \psi_i^h \left|h, i\right\rangle. \tag{4}$$

Proof. Assume that

$$\left|\text{IGC}\right\rangle = \sum_i \psi_i^h \left|h, i\right\rangle + \sum_j \psi_j^{nh} \left|nh, j\right\rangle. \tag{5}$$

Then

$$\left\langle\text{IGC}\right| (H - H^\dagger) \left|\text{IGC}\right\rangle = -2i \sum_j \gamma_j \left|\psi_j^{nh}\right|^2, \tag{6}$$

where $-\gamma_j = \text{Im}(b_{jj})$ is the dissipative rate of site (nh, j), and $\gamma_j > 0$. Notice that the left-hand side of Eq. (6) also equals to

$$\left\langle\text{IGC}\right| (H - H^\dagger) \left|\text{IGC}\right\rangle = E_{\text{IGC}} - E_{\text{IGC}}^* = 0. \tag{7}$$

So $\psi_j^{nh} = 0$ for all (nh, j) sites. ■

Lemma 1 aligns well with our physical intuition. If an eigenstate has a population on dissipative sites, then the norm of the eigenstate will decrease with time, which implies the presence of an imaginary part in the energy. Via Lemma 1, the eigenequation of IGC states becomes

$$\begin{aligned} 0 &= (H - E_{\text{IGC}}) \left|\text{IGC}\right\rangle \\ &= (H_h - E_{\text{IGC}}) \left|\text{IGC}\right\rangle + H_{\text{inter}} \left|\text{IGC}\right\rangle. \end{aligned} \tag{8}$$

Notice that $(H_h - E_{\text{IGC}}) \left|\text{IGC}\right\rangle$ is only populated on nondissipative sites, while $H_{\text{inter}} \left|\text{IGC}\right\rangle$ is only populated on dissipative sites. Hence, Eq. (8) can be decomposed into two separate parts

$$(H_h - E_{\text{IGC}}) \left|\text{IGC}\right\rangle = 0, \quad H_{\text{inter}} \left|\text{IGC}\right\rangle = 0. \tag{9}$$

This implies that IGC states not only belong to the kernel of H_{inter} but also function as eigenstates of a system solely comprised of nondissipative sites, retaining their original eigenvalues. The term H_{inter} can be interpreted as a representation of the coupling between nondissipative and dissipative sites. Equation (9) signifies that upon connecting the nondissipative subsystem to the dissipative subsystem, these IGC states remain eigenstates of the combined system with their eigenvalues preserved.

In summary, IGC states can be described as dark modes characterized by the absence of a population on dissipative sites. Notably, IGC states are the eigenstates of H_h, satisfying the connection conditions H_{inter}, independent of H_{nh}. Our findings hold true for a broad class of systems, as evidenced by their applicability to arbitrary Hamiltonian that only have non-Hermitian terms on its diagonal like Eq. (2). However, limitations arise when considering effective Hamiltonians with off-diagonal non-Hermitian terms. These nondiagonal forms, often encountered in systems like atoms coupled by the

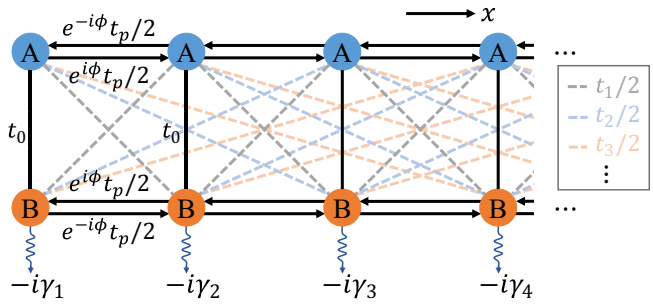

FIG. 2. Model of the one-dimensional dissipative ladder. Each unit cell is labeled by spatial coordinate x and contains two sites, A and B. The non-Hermiticity comes from site-dependent decay γ_x.

electromagnetic field [105–107], whose dissipative dynamics can lead to phenomena like fluorescence [108], superradiance [109–111], and subradiance [112]. Our current theory necessitates further development to encompass these phenomena effectively.

III. IMAGINARY GAPLESS MODES AND DYNAMICS OF QUANTUM WALK

To investigate the impact of IGC modes on dynamical evolution, we delve into a more concrete model and analyze its quantum walk behavior. We consider a one-dimensional tight-binding model on a dissipative ladder of length L, as shown in Fig. 2. The A-B coupling range is n, meaning particles can hop between different sublattices up to the nth-nearest unit cells. Hopping along the same chain carries a Peierls phase ϕ [113,114], which induces gauge fluxes in closed hopping contours and breaks the time-reversal symmetry of the system. The non-Hermiticity comes from the site-dependent dissipation γ_x, which induces the NHSE under OBC [115]. Then, we check the IGC states of this system under PBC. According to Eq. (9), IGC states of this system are also the eigenstates of chain A, given by

$$|\mathrm{IGC}\rangle = \frac{1}{\sqrt{L}} \sum_{x=1}^{L} e^{ikx} |x, A\rangle . \tag{10}$$

These states possess eigenenergies

$$E_{\mathrm{IGC}} = t_p \cos(k - \phi), \tag{11}$$

where $k = 2\pi n/L$ with $n = 0, 1, 2, \ldots, L-1$.

The specific value of k is determined by the connection condition obtained in Eq. (9):

$$\sum_{m=0}^{n} t_m \cos(mk) = 0. \tag{12}$$

At $k = 0$, the left-hand side of Eq. (12), denoted as $F(k)$, attains its maximum value $\sum_{m=0}^{n} t_m > 0$. So, if the minimum value of $F(k)$ is smaller than or equal to zero, Eq. (12) has real roots, and the energy spectrum is IGC. In finite chains, satisfying condition (12) with a discrete crystal momentum k might not be achievable. However, from a dynamical perspective, their bulk dynamical behavior mirrors that of the infinite-chain limit due to the local nature of propagation. Treating k as continuous in this limit enables the identification of rigorous IGC points.

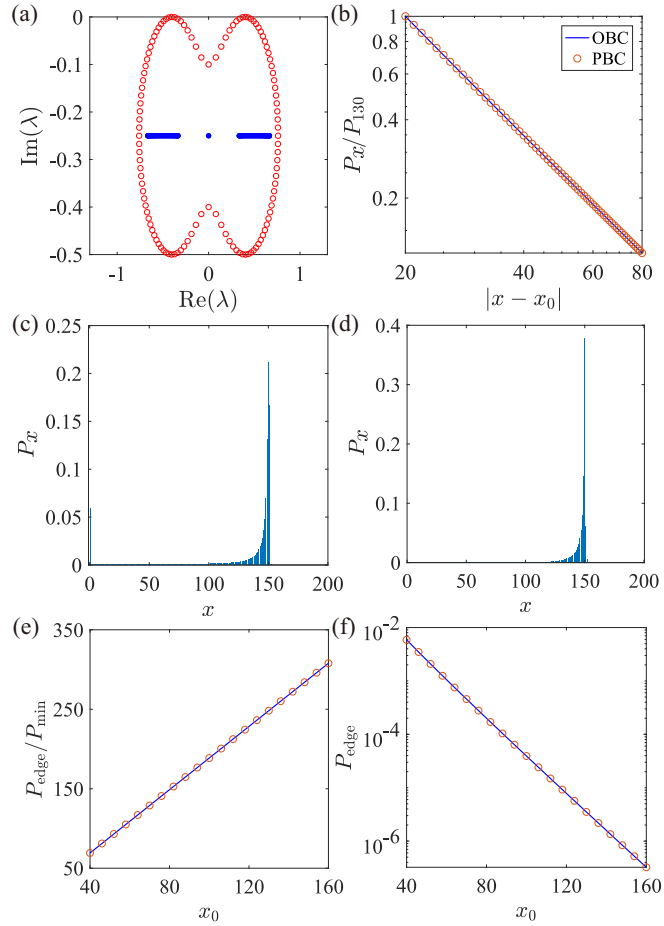

FIG. 3. The model with only the nearest A-B coupling (a) energy spectra with $t_0 = 0.3$. Blue: OBC; red: PBC. (b) The bulk distribution of the relative loss probabilities P_x/P_{130} in a double-logarithmic plot with $t_0 = 0.3$ for system size $L = 200$, initial position $x_0 = 150$. (c), (d) The distribution of P_x for a walker initiated at $x_0 = 150$ with $L = 200$ under OBC. $t_0 = 0.3$ for (c) and $t_0 = 0.6$ for (d). (e) Relative height $P_{\mathrm{edge}}/P_{\mathrm{min}}$ and (f) the edge loss probability P_{edge} with chain length $L = 200$, and x_0 varying from 40 to 160. $t_0 = 0.3$ for (c) and $t_0 = 0.6$ for (d) in a logarithmic plot. Throughout (a)–(f), $\phi = \pi/2$, $t_1 = 0.5$, $t_p = 0.5$, and $\gamma = 0.5$ are fixed.

Notably, the system under OBC lacks IGC states. This is because any IGC state would also be an eigenstate of the Hermitian H_h, which is an extended state, contradicting the NHSE's localized nature under OBC. Alternatively, in systems with the NHSE, OBC spectra are enclosed by their PBC counterparts [91,102]. For this dissipative lattice, the PBC spectra maximum imaginary part is zero, rendering the OBC spectra always imaginary gapped. An example is shown in Fig. 3(a).

Although substantial differences exist in the spectrum and eigenstates between OBC and PBC for this model, the dynamics within the bulk exhibit similarity for both cases. This similarity is evident from the Schrödinger equation $i(d/dt)|\psi(t)\rangle = H|\psi(t)\rangle$ (we set $\hbar = 1$ throughout this paper). Under PBC, the Hamiltonian is given by

$H_{\mathrm{PBC}} = H_{\mathrm{OBC}} + \delta H$. Here, δH represents the coupling term that connects the two boundaries. When a wave function $|\psi(t)\rangle$ predominantly resides in the bulk, with negligible population at the boundaries, $\delta H\,|\psi(t)\rangle \approx 0$, and then consequently, the Schrödinger equations for OBC and PBC become effectively equivalent in this approximation. This feature is exemplified in Fig. 3(b). In the following, we show that the dynamical evolution properties of quantum walks under OBCs can be elucidated by IGC points of the PBC spectra.

Considering a quantum walk in this model under OBC, a particle is released at the site (x_0, A). Subsequently, the particle's wave function diffuses from the initial location (x_0, A) and escapes from lossy B sites. The wave-function norm decreases as

$$\frac{d}{dt}\langle\psi(t)|\psi(t)\rangle = i\big\langle\psi(t)|(H^\dagger - H)|\psi(t)\big\rangle = -\sum_x 2\gamma_x|\psi_x^B(t)|^2. \tag{13}$$

The escape probability from site (x, B) is employed to characterize this quantum walk, given by

$$P_x = 2\gamma_x\int_0^\infty \left|\psi_x^B(t)\right|^2 dt. \tag{14}$$

Then, we can use the non-Hermitian Green's function [104] to express P_x as

$$P_x = \gamma_x\int_{-\infty}^{+\infty}\frac{d\omega}{\pi}\left|\langle x, B\left|\frac{1}{\omega - H}\right|x_0, A\rangle\right|^2. \tag{15}$$

Note that $\Sigma_x P_x = 1$ is satisfied under the initial-state normalization $\langle\psi(0)|\psi(0)\rangle = 1$. Intuitively, the distribution P_x features a peak centered on the site x_0, displaying left-right asymmetry attributable to the NHSE, which causes the wave function to move leftward preferentially [116]. However, under certain parameters, a prominent peak, named edge burst, emerges at the left edge [117]. In a recent paper, Xue *et al.* investigated this model with the nearest A-B hopping term and uniform dissipation, i.e., γ_x is a constant, revealing that the edge burst phenomenon results from the interplay between the IGC spectrum under PBC and the NHSE [104].

When there are IGC states, the escape probability P_x decays slowly as a power law with the distance from the initial position x_0,

$$P_x \sim |x - x_0|^{-\alpha_b}. \tag{16}$$

In this case, the walker remains a large wave-function amplitude when it arrives at the left edge [118]. Then, the walker becomes trapped due to the NHSE and escapes from $(1, B)$ site over time, leading to a high peak P_{edge}, as shown in Fig. 3(c). If we shift the left boundary to infinite, the walker is no longer localized at $x = 1$ and carries out left walking quickly through this position, resulting in a tiny P_1. This argument gives an estimation of P_{edge} as follows:

$$P_{\mathrm{edge}} \sim \sum_{-\infty}^{0} P_x \sim \int_{-\infty}^{0}|x - x_0|^{-\alpha_b}dx \sim (x_0)^{-\alpha_b+1}. \tag{17}$$

Here, we have assumed that bulk P_x is only determined by the relative distance to the initial position x_0, and system-size effects can be neglected. On the other hand, Eq. (16) implies that P_x takes the minimum near the edge, which gives the estimation $P_{\mathrm{min}} \sim x_0^{-\alpha_b}$. Therefore, it follows from Eq. (17) that

$$P_{\mathrm{edge}}/P_{\mathrm{min}} \sim x_0, \tag{18}$$

which can be confirmed by our numerical results shown in Fig. 3(e). Thus, if the initial position x_0 is far from the edge, there is a large peak P_{edge} compared to almost invisible P_x in the vicinity sites.

In contrast, when there are no IGC states, bulk P_x decays fast as exponential law with

$$P_x \sim (\lambda_b)^{x_0 - x} \quad (\lambda_b < 1). \tag{19}$$

In this case, wave-function amplitude becomes very small when the walker arrives at the left edge. Similarly, we have the estimation

$$P_{\mathrm{edge}} \sim \sum_{-\infty}^{0} P_x \sim \int_{-\infty}^{0}(\lambda_b)^{x_0 - x}dx \sim (\lambda_b)^{x_0}. \tag{20}$$

P_{edge} is of the same order as the decay tail and, therefore, as shown in Fig. 3(d), no edge burst exists. The relationship between P_{edge} and x_0 in Eq. (20) is verified by the numerical results shown in Fig. 3(f).

IV. IMPACT OF PARAMETERS

The above discussion shows that IGC points of PBC spectra are crucial to the non-Hermitian dynamics. In this section, we explore the quantum walk across various parameters, demonstrating the universality of the correlation between edge burst and IGC points. This correlation remains independent of the values or distribution of A-B hopping terms, Peierls phases, and loss rates. This indicates that the bulk dynamics can be effectively captured in these models by specific spectra characteristics under PBCs.

A. *A-B* coupling model second-nearest intercell hopping

In this subsection, we consider the impact of A-B hopping terms with long range. For concreteness, the intercell A-B coupling extends to the second-nearest neighbor, and the Peierls phase takes $\phi = \pi/2$. Additionally, a uniform loss rate of γ is applied. The Bloch Hamiltonian is given by

$$H(k) = h_x(k)\sigma_x + \left(h_y(k) + i\frac{\gamma}{2}\right)\sigma_z - i\frac{\gamma}{2}I, \tag{21}$$

where $h_x(k) = t_0 + t_1\cos k + t_2\cos 2k$, $h_y(k) = t_p\sin k$, and $\sigma_{x,z}$ are the Pauli matrices. Since $h_x(k) = F(k)$, the IGC points are determined by $h_x(k) = 0$. This condition, expressed in terms of the Bloch phase factor $\beta = e^{ik}$, becomes

$$t_0 + \frac{t_1}{2}(\beta + \beta^{-1}) + \frac{t_2}{2}(\beta^2 + \beta^{-2}) = 0. \tag{22}$$

This is a quartic equation of β with the constraint $|\beta| = 1$. Therefore, the maximum number of IGC points is four, which is confirmed by the numerical results of the energy spectra. Furthermore, we can infer that if intercell A-B couplings are up to the nth-nearest neighbors, the maximum number of IGC points is $2n$.

As $h_x(0) = t_0 + t_1 + t_2 > 0$ [maximum value of $h_x(k)$], the existence of IGC points solely depends on the minimum value

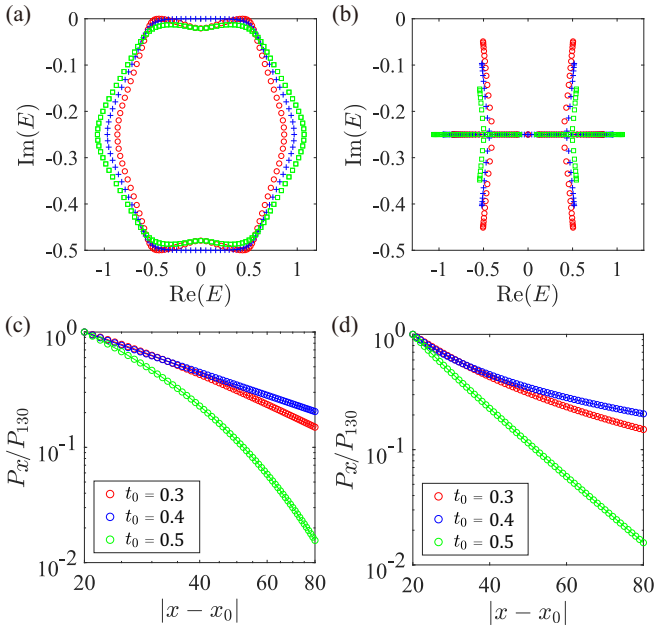

FIG. 4. (a), (b) Energy spectra under (a) PBCs and (b) OBCs, $t_0 = 0.3$ (red), 0.4 (blue), and 0.5 (green). (c), (d) The bulk distribution of P_x in double-logarithmic (c) and logarithmic (d) plots. System size $L = 200$, and the initial position $x_0 = 150$. Throughout (a)–(d), $t_p = 0.5, t_1 = 0.5, t_2 = 0.1, \gamma = 0.5$ are fixed.

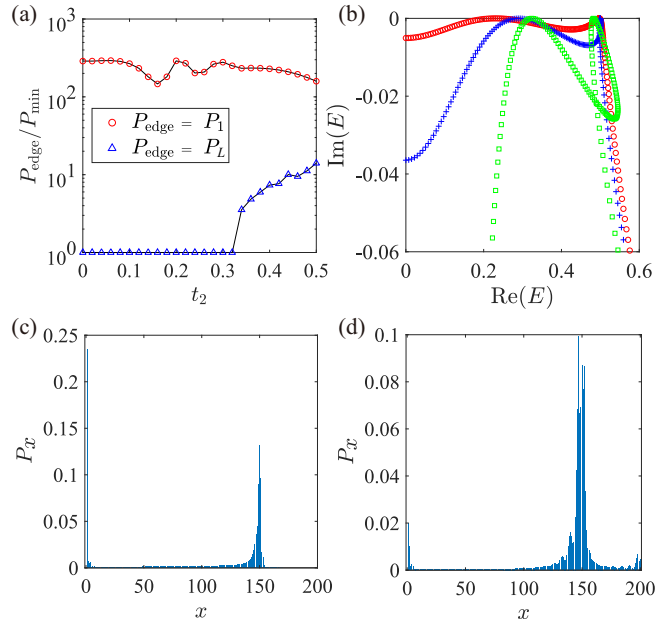

FIG. 5. (a) The relative height $P_{\text{edge}}/P_{\min}$ with varying t_2. (b) Part of the energy spectra with system size $L = 500$ under PBCs, $t_2 = 0.25$ (red), 0.33 (blue), and 0.50 (green) (c), (d) The loss probability P_x for a walker initiated at $x_0 = 150$ with $L = 200$. $t_2 = 0.2$ for (c) and $t_2 = 0.5$ for (d). Throughout (a)–(d), $t_p = 0.5$, $t_0 = 0.3$, $t_1 = 0.5, \gamma = 0.5$ are fixed.

$h_x(k_0)$. By analyzing $h_x(k)$, we find that the expression for $h_x(k_0)$ takes a different form when the parameters change. When $t_2 \leqslant t_1/4$, $h_x(k_0)$ is given by

$$h_x(k_0) = t_0 - t_1 + t_2, \tag{23}$$

with $k_0 = \pi$. Conversely, for $t_2 > t_1/4$, the expression changes to

$$h_x(k_0) = t_0 - \frac{t_1^2}{8t_2} - t_2, \tag{24}$$

with $\cos k_0 = -t_1/4t_2$. Combining Eqs. (23) and (24), we obtain the maximum value of $h_x(k_0)$ as $t_0 - (t_1/\sqrt{2})$, achieved when $t_2 = t_1/2\sqrt{2}$. Thus, the inequality $h_x(k_0) \leqslant 0$ always holds in the regime $t_0 \leqslant t_1/\sqrt{2}$, regardless of the value of t_2. Consequently, the energy spectra of the Bloch Hamiltonian (21) are guaranteed to exhibit IGC points. However, for $t_0 > t_1/\sqrt{2}$, the existence of IGC points becomes contingent on specific values of hopping parameters t_0, t_1, and t_2. For example, as shown in Fig. 4(a), when fixing other parameters and increasing the parameter t_0, two IGC points gradually close together. At a critical value, they merge into a single IGC point. Besides, no IGC points exist when t_0 exceeds this critical value. Apparently, the corresponding OBC spectra do not have IGC points, which is shown in Fig. 4(b). As discussed in Sec. III, whether energy spectra have IGC points can be linked to the quantum walk behavior. Figures 4(c) and 4(d) illustrate this connection, where the bulk distribution of particle loss probabilities P_x exhibits power-law behavior for PBC spectra with IGC points and exponential behavior for spectra without them.

To demonstrate the feature of the edge burst phenomenon for this model, we choose specific parameter values $t_0 = 0.3$ and $t_1 = 0.5$. As previously established, the IGC condition is automatically satisfied because the maximum value of $h_x(k_0)$ is strictly negative. The relative heights $P_{\text{edge}}/P_{\min}$ are vital to depict edge burst, as these physical quantities are closely related to the decay scaling behavior of the walker in the bulk. Here, P_{edge} are the escape probabilities at two edges and equal to P_1 or P_L. $P_{\min}$ is defined as $\min\{P_1, P_2, \ldots, P_{x_0}\}$ for $P_{\text{edge}} = P_1$ and $\min\{P_{x_0}, P_{x_0+1}, \ldots, P_L\}$ for $P_{\text{edge}} = P_L$. We calculate $P_{\text{edge}}/P_{\min}$ as the parameter t_2 increasing from zero [see Fig. 5(a)]. For small t_2, the ratio $P_1/P_{\min} \gg 1$ while $P_L/P_{\min} \sim 1$, which indicates a single remarkable probability loss peak at the left edge [Fig. 5(c)]. As t_2 exceeds a critical value, $P_L/P_{\min}$ increases rapidly and becomes much larger than one. In this case, the system exhibits two remarkable probability loss peaks at both left and right edges [Fig. 5(d)]. This phenomenon is closely linked to the bipolar skin effect, which corresponds to the self-intersecting point of the PBC spectrum [119] [see green line in Fig. 5(b)]. Another interesting aspect of the edge burst phenomenon is that the ratio of P_1/P_{x_0} can be greater than 1 [see Fig. 5(c)], which is not observed in the system for $t_2 = 0$.

B. Model with varying Peierls phases ϕ

In this subsection, we focus on the influence of the Peierls phase ϕ. For simplicity, we only consider the nearest-neighbor intercell A-B coupling with uniform loss rate γ, and the Bloch Hamiltonian is

$$H(k) = (t_0 + t_1 \cos k)\sigma_x + \left[t_p \cos(k - \phi) + i\frac{\gamma}{2}\right]\sigma_z - i\frac{\gamma}{2}I. \tag{25}$$

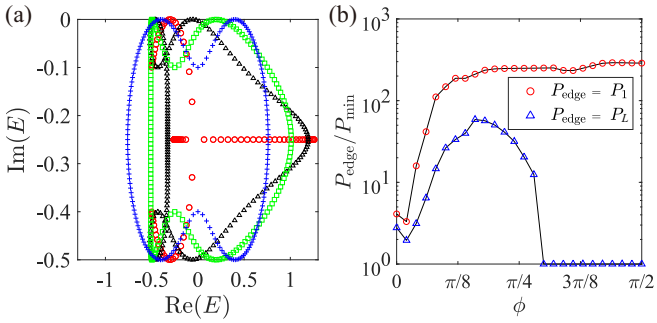

FIG. 6. (a) Energy spectra under PBCs. Peierls phases ϕ are set to 0 (red), $\pi/6$ (black), $\pi/3$ (green), and $\pi/2$ (blue). (b) The relative height $P_{\text{edge}}/P_{\text{min}}$ with varying ϕ. System size $L = 200$ and initial position $x_0 = 150$. Throughout (a) and (b), $t_p = 0.5$, $t_0 = 0.3$, $t_1 = 0.5$, $\gamma = 0.5$ are fixed.

IGC points are given by $t_0 + t_1 \cos k = 0$. The eigenvalues of IGC states described by Eq. (11) can be expressed in terms of the system parameters as follows:

$$E_{\text{IGC}} = \frac{t_p}{t_1}\big(-t_0 \cos\phi \pm \sqrt{t_1^2 - t_0^2}\sin\phi\big). \tag{26}$$

This analytical expression exhibits good agreement with numerical results of energy spectra under PBCs, as shown in Fig. 6(a). Therefore, Peierls phases ϕ do not alter the IGC conditions or impact the bulk scaling behavior of P_x. They only shift the values of E_{IGC} along the real axis.

When $\phi = 0$, the Hermitian part of the Bloch Hamiltonian (25) has time-reversal symmetry. Consequently, the onsite dissipation does not induce the NHSE. In this case, the distribution of P_x is left-right symmetric, and there is no edge burst phenomenon. As ϕ increases from zero, this model breaks time-reversal symmetry and thus features the NHSE. We can see from Fig. 6(b) that the quantum walk exhibits a bipolar edge burst for a not very large ϕ and reduces to a standard edge burst on the left side when it exceeds some critical value. The corresponding PBC spectra also exhibit the emergence and disappearance of self-intersecting points, as shown in Fig. 6(a).

C. Model with varying loss rate γ_x

In this subsection, we discuss the effect of loss rate distribution. We focus on the model with nearest-neighbor intercell A-B coupling and $\phi = \pi/2$ for convenience. The system breaks discrete translational symmetry if the loss rate γ_x is not uniform. Thus, the Hamiltonian under PBC cannot be expressed in a simple Bloch form, and eigenstates cease to be Bloch waves. However, as established in Sec. II, IGC states exhibit invariance, remaining unaffected by the specific form of γ_x. Let us consider a linear form of γ_x as follows:

$$\gamma_x = \gamma_0 x + \gamma_c. \tag{27}$$

As shown in Fig. 7(a), this nonuniform system transitions from IGC to imaginary gapped when increasing the value of t_0. IGC points of the PBC spectra also determine the bulk dynamics of quantum walk in this nonuniform system. When IGC points exist, P_x follows a power-law decay in the bulk. Conversely, in the absence of points, P_x follows an exponential

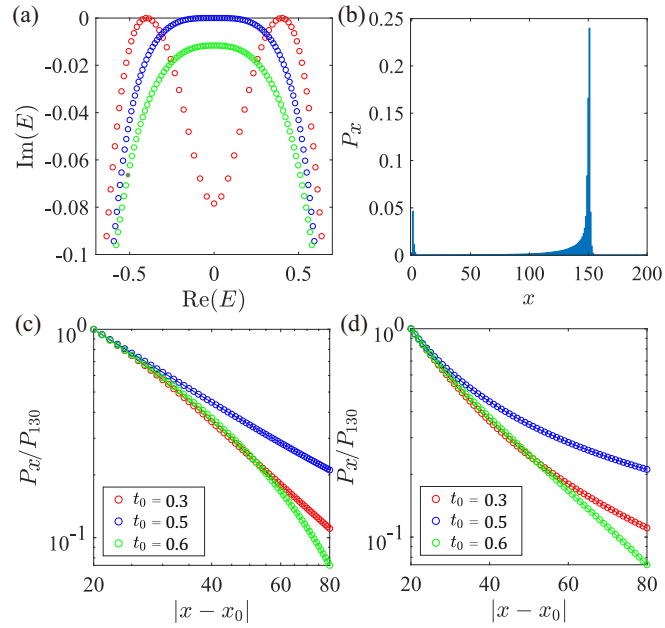

FIG. 7. (a) Energy spectra under PBCs. $t_0 = 0.3$ (red), $t_0 = 0.5$ (blue), $t_0 = 0.6$ (green). (b) The distribution of P_x when $t_0 = 0.3$. (c), (d) The bulk distribution of P_x in double-logarithmic (c) and logarithmic (d) plots with nonuniform loss rates. For (b)–(d), system size $L = 200$ and the initial position $x_0 = 150$. Throughout (a)–(d), $t_p = 0.5$, $t_1 = 0.5$, $\gamma_0 = 0.01$, $\gamma_c = 0.20$ are fixed.

law decay in the bulk. We can see this clearly in Figs. 7(c) and 7(d). Besides, a remarkable probability loss peak appeared at the edge when bulk P_x shows a power-law decay, as shown in Fig. 7(b). This gives an explicit explanation of the edge burst phenomenon in Ref. [120].

V. RELATION TO THE LIOUVILLIAN DYNAMICS

Leveraging the established correspondence between non-Hermitian dynamics and steady states of open quantum systems (as explored in Ref. [121]), our conclusions can be generalized to open quantum systems as well. When a quantum system is coupled to a Markovian bath, the corresponding dynamical evolution of the density matrix is governed by the master equation, which can be expressed in Lindblad formalism [21]

$$\frac{d\rho}{dt} = -i[H_0, \rho] + \sum_\alpha (2L_\alpha \rho L_\alpha^\dagger - \{L_\alpha^\dagger L_\alpha, \rho\}), \tag{28}$$

where H_0 is the Hamiltonian of the system, L_α are the Lindblad dissipators describing quantum jumps randomly moving the state $|\psi\rangle$ to $L_\alpha|\psi\rangle$. In this system, the quantum dynamics started from single-particle states are controlled by the effective Hamiltonian $\mathcal{H}_{\text{eff}} = H_0 - i\sum_\alpha L_\alpha^\dagger L_\alpha$ as $d\rho/dt = i(\rho\mathcal{H}_{\text{eff}}^\dagger - \mathcal{H}_{\text{eff}}\rho)$.

In the open chain, we consider [Fig. 8(a)], the dissipators are given by $L_x = \sqrt{\gamma_x} c_x^{\text{B}}$. Notably, the long-time evolution of the system can be captured by the single-particle correlation function $C_{xy}(t) = \text{Tr}[\rho(t) c_x^\dagger c_y]$. For this dissipative system, any initial state will converge to the nonequilibrium steady-state correlation $C(\infty)$, determined by $dC(\infty)/dt = 0$. In this

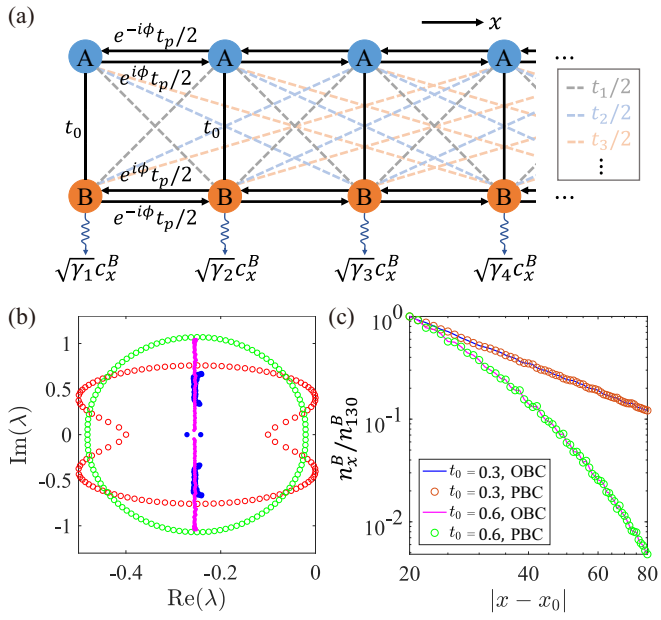

FIG. 8. (a) The corresponding bosonic quadratic open quantum system. (b), (c) The model only considers the nearest A-B coupling and chooses $\phi = \pi/2$, $t_1 = 0.5$, $t_p = 0.5$, and $0.4 < \gamma_x < 0.6$ (randomly distributed). (b) Liouvillian spectra. Blue: OBC, $t_0 = 0.3$; red: PBC, $t_0 = 0.3$; purple: OBC, $t_0 = 0.6$; green: PBC, $t_0 = 0.6$. (c) The bulk distribution of P_x in a double-logarithmic plot.

paper, we mainly consider the speed of converging to the steady state and focus on the deviation $\tilde{C}(t) = C(t) - C(\infty)$, whose evolution equation is given by

$$\frac{d}{dt}\tilde{C}(t) = X\tilde{C}(t) + \tilde{C}(t)X^\dagger, \tag{29}$$

where the damping matrix $X = i(H_0^T + iM)$ and directly connects to the non-Hermitian Hamiltonian H in real space as $X = iH^*$. Here, M is a diagonal matrix whose diagonal elements are $\{0, \gamma_1, 0, \gamma_2, \ldots, 0, \gamma_n\}$. The solution of $\tilde{C}$ is

$$\tilde{C}(t) = e^{Xt}\tilde{C}(0)e^{X^\dagger t}. \tag{30}$$

By expressing X in terms of right and left eigenvectors,

$$X = \sum_n \lambda_n |\psi_n\rangle\langle\phi_n|, \tag{31}$$

we can write Eq. (30) as

$$\tilde{C}(t) = \sum_{n,n'} \exp[(\lambda_n + \lambda_{n'}^*)t]|\psi_n\rangle\langle\phi_n|\tilde{C}(0)|\phi_{n'}\rangle\langle\psi_{n'}|. \tag{32}$$

Due to the dissipative nature of the system, $\mathrm{Re}(\lambda_n) \leqslant 0$ always holds. The Liouvillian gap is defined as $\Delta = \min[2\,\mathrm{Re}(-\lambda_n)]$, which is crucial to the long-time dynamics. A finite gap implies exponential convergence towards the steady state, while a vanishing gap implies algebraic convergence [93,122].

Using a method similar to Sec. II, we can demonstrate that the damping matrix X of the open chain under PBC also has universal Liouvillian gapless points. We can check our conclusion numerically with a specific model. Let the hopping $t_m = 0$, $m = 2, 3, \ldots$, we can take the distribution of dissipators to be randomly distributed, namely, $L_x = \sqrt{\gamma_x}c_x^B$, where γ_x is a random number within 0.4 and 0.6, it varies for each x. And we get the Liouvillian spectrum [Fig. 8(b)]. We can see that if the condition of Eq. (12) can be satisfied, the Liouvillian spectrum can have Liouvillian gapless points, which correspond to the eigenmodes of the form $(1, 0, e^{ik}, 0, e^{i2k}, 0, \ldots, e^{ikN}, 0)$. These modes can be viewed as dark modes, which lead to the algebraic convergence towards the steady state in the bulk [Fig. 8(c)]. Here, we already replaced the loss probability on B sites P_x with the steady-state density on B sites n_x^B, which can be written as [121]

$$n_x^B = [C(\infty)]_{xB,xB} = \gamma_x \int_{-\infty}^{+\infty} \frac{d\omega}{\pi} |\langle xB| \frac{1}{i\omega - X} |x_0 A\rangle|^2. \tag{33}$$

Comparing Eqs. (15) and (33), we can find the equivalence between the loss probability P_x and the steady-state density n_x^B. Results show that the Liouvillian gapless points are indeed only related to the properties of Hermitian Hamiltonian under PBC and irrelevant to the dissipation of the system.

VI. SUMMARY

In summary, our investigation centers on IGC points and relative dynamic characteristics in dissipative systems. For the onsite dissipative non-Hermitian model, we deduce the equation governing the IGC points. This analysis reveals that IGC states are unaffected by the non-Hermitian part of the Hamiltonian and serve as dark modes characterized by the absence of a population on dissipative sites. Then, we examine quantum walks across diverse scenarios and parameters for a class of one-dimensional dissipative chains, highlighting the pivotal role of IGC points under PBC in shaping quantum walk dynamics. Finally, we show that the PBC damping matrix of the dissipative chain can exhibit Liouvillian gapless points, which correspond to an algebraic convergence towards the steady state in long-time dynamics. As the onsite dissipation is feasible to implement, our theory of IGC points can be confirmed in various non-Hermitian platforms, for example, the photon quantum walk [123], dissipative cold-atom systems [124], and nuclear spin systems [125].

ACKNOWLEDGMENTS

The authors would like to thank P. Wen and Y. Qi for their helpful discussion. This work is supported by the National Natural Science Foundation of China under Grants No. 11974205 and No. 61727801, and the Key Research and Development Program of Guangdong province (Grant No. 2018B030325002).

[1] H. Cao and J. Wiersig, Dielectric microcavities: Model systems for wave chaos and non-Hermitian physics, Rev. Mod. Phys. **87**, 61 (2015).

[2] V. V. Konotop, J. Yang, and D. A. Zezyulin, Nonlinear waves in $\mathcal{PT}$-symmetric systems, Rev. Mod. Phys. **88**, 035002 (2016).

[3] R. El-Ganainy, K. G. Makris, M. Khajavikhan, Z. H. Musslimani, S. Rotter, and D. N. Christodoulides, Non-Hermitian physics and pt symmetry, Nat. Phys. **14**, 11 (2018).

[4] Y. Ashida, Z. Gong, and M. Ueda, Non-Hermitian physics, Adv. Phys. **69**, 249 (2020).

[5] E. J. Bergholtz, J. C. Budich, and F. K. Kunst, Exceptional topology of non-Hermitian systems, Rev. Mod. Phys. **93**, 015005 (2021).

[6] N. Okuma and M. Sato, Non-Hermitian topological phenomena: A review, Annu. Rev. Condens. Matter Phys. **14**, 83 (2023).

[7] K. G. Makris, R. El-Ganainy, D. N. Christodoulides, and Z. H. Musslimani, Beam dynamics in $\mathcal{PT}$ symmetric optical lattices, Phys. Rev. Lett. **100**, 103904 (2008).

[8] A. Mostafazadeh, Spectral singularities of complex scattering potentials and infinite reflection and transmission coefficients at real energies, Phys. Rev. Lett. **102**, 220402 (2009).

[9] C. E. Rüter, K. G. Makris, R. El-Ganainy, D. N. Christodoulides, M. Segev, and D. Kip, Observation of parity–time symmetry in optics, Nat. Phys. **6**, 192 (2010).

[10] S. Longhi, $\mathcal{PT}$-symmetric laser absorber, Phys. Rev. A **82**, 031801(R) (2010).

[11] Y. D. Chong, L. Ge, and A. D. Stone, $\mathcal{PT}$-symmetry breaking and laser-absorber modes in optical scattering systems, Phys. Rev. Lett. **106**, 093902 (2011).

[12] Z. Lin, H. Ramezani, T. Eichelkraut, T. Kottos, H. Cao, and D. N. Christodoulides, Unidirectional invisibility induced by $\mathcal{PT}$-symmetric periodic structures, Phys. Rev. Lett. **106**, 213901 (2011).

[13] A. Regensburger, C. Bersch, M.-A. Miri, G. Onishchukov, D. N. Christodoulides, and U. Peschel, Parity–time synthetic photonic lattices, Nature (London) **488**, 167 (2012).

[14] L. Feng, Y.-L. Xu, W. S. Fegadolli, M.-H. Lu, J. E. Oliveira, V. R. Almeida, Y.-F. Chen, and A. Scherer, Experimental demonstration of a unidirectional reflectionless parity-time metamaterial at optical frequencies, Nat. Mater. **12**, 108 (2013).

[15] B. Peng, Ş. K. Özdemir, F. Lei, F. Monifi, M. Gianfreda, G. L. Long, S. Fan, F. Nori, C. M. Bender, and L. Yang, Parity–time-symmetric whispering-gallery microcavities, Nat. Phys. **10**, 394 (2014).

[16] B. Peng, Ş. K. Özdemir, S. Rotter, H. Yilmaz, M. Liertzer, F. Monifi, C. M. Bender, F. Nori, and L. Yang, Loss-induced suppression and revival of lasing, Science **346**, 328 (2014).

[17] H. Hodaei, M.-A. Miri, M. Heinrich, D. N. Christodoulides, and M. Khajavikhan, Parity-time symmetric microring lasers, Science **346**, 975 (2014).

[18] J. Wiersig, Enhancing the sensitivity of frequency and energy splitting detection by using exceptional points: Application to microcavity sensors for single-particle detection, Phys. Rev. Lett. **112**, 203901 (2014).

[19] H. Hodaei, A. U. Hassan, S. Wittek, H. Garcia-Gracia, R. El-Ganainy, D. N. Christodoulides, and M. Khajavikhan, Enhanced sensitivity at higher-order exceptional points, Nature (London) **548**, 187 (2017).

[20] W. Chen, Ş. Kaya Özdemir, G. Zhao, J. Wiersig, and L. Yang, Exceptional points enhance sensing in an optical microcavity, Nature (London) **548**, 192 (2017).

[21] G. Lindblad, On the generators of quantum dynamical semigroups, Commun. Math. Phys. **48**, 119 (1976).

[22] J. Dalibard, Y. Castin, and K. Mølmer, Wave-function approach to dissipative processes in quantum optics, Phys. Rev. Lett. **68**, 580 (1992); K. Mølmer, Y. Castin, and J. Dalibard, Monte carlo wave-function method in quantum optics, J. Opt. Soc. Am. B **10**, 524 (1993).

[23] R. Dum, P. Zoller, and H. Ritsch, Monte Carlo simulation of the atomic master equation for spontaneous emission, Phys. Rev. A **45**, 4879 (1992).

[24] H. Carmichael, *An open systems approach to quantum optics* (Springer, Berlin, 1993).

[25] M. B. Plenio and P. L. Knight, The quantum-jump approach to dissipative dynamics in quantum optics, Rev. Mod. Phys. **70**, 101 (1998).

[26] A. J. Daley, Quantum trajectories and open many-body quantum systems, Adv. Phys. **63**, 77 (2014).

[27] G. Gamow, Zur quantentheorie des atomkernes, Z. Phys. **51**, 204 (1928).

[28] H. Feshbach, C. E. Porter, and V. F. Weisskopf, Model for nuclear reactions with neutrons, Phys. Rev. **96**, 448 (1954); H. Feshbach, Unified theory of nuclear reactions, Ann. Phys. **5**, 357 (1958). A unified theory of nuclear reactions. II, **19**, 287 (1962).

[29] I. Rotter, A non-Hermitian hamilton operator and the physics of open quantum systems, J. Phys. A: Math. Theor. **42**, 153001 (2009).

[30] N. Moiseyev, *Non-Hermitian Quantum Mechanics* (Cambridge University Press, Cambridge, 2011)

[31] P. Peng, W. Cao, C. Shen, W. Qu, J. Wen, L. Jiang, and Y. Xiao, Anti-parity–time symmetry with flying atoms, Nat. Phys. **12**, 1139 (2016).

[32] J. Li, A. K. Harter, J. Liu, L. de Melo, Y. N. Joglekar, and L. Luo, Observation of parity-time symmetry breaking transitions in a dissipative floquet system of ultracold atoms, Nat. Commun. **10**, 855 (2019).

[33] Z. Ren, D. Liu, E. Zhao, C. He, K. K. Pak, J. Li, and G.-B. Jo, Chiral control of quantum states in non-Hermitian spin–orbit-coupled fermions, Nat. Phys. **18**, 385 (2022).

[34] L. Xiao, X. Zhan, Z. Bian, K. Wang, X. Zhang, X. Wang, J. Li, K. Mochizuki, D. Kim, N. Kawakami *et al.*, Observation of topological edge states in parity–time-symmetric quantum walks, Nat. Phys. **13**, 1117 (2017).

[35] K. Kawabata, Y. Ashida, and M. Ueda, Information retrieval and criticality in parity-time-symmetric systems, Phys. Rev. Lett. **119**, 190401 (2017); L. Xiao, K. Wang, X. Zhan, Z. Bian, K. Kawabata, M. Ueda, W. Yi, and P. Xue, Observation of critical phenomena in parity-time-symmetric quantum dynamics, *ibid.* **123**, 230401 (2019).

[36] B. Dóra, M. Heyl, and R. Moessner, The kibble-zurek mechanism at exceptional points, Nat. Commun. **10**, 2254 (2019); L. Xiao, D. Qu, K. Wang, H.-W. Li, J.-Y. Dai, B. Dóra, M. Heyl, R. Moessner, W. Yi, and P. Xue, Non-Hermitian kibble-zurek mechanism with tunable complexity in single-photon interferometry, PRX Quantum **2**, 020313 (2021).

[37] F. E. Öztürk, T. Lappe, G. Hellmann, J. Schmitt, J. Klaers, F. Vewinger, J. Kroha, and M. Weitz, Observation of a non-Hermitian phase transition in an optical quantum gas, Science **372**, 88 (2021).

[38] T. Gao, E. Estrecho, K. Bliokh, T. Liew, M. Fraser, S. Brodbeck, M. Kamp, C. Schneider, S. Höfling, Y. Yamamoto *et al.*, Observation of non-Hermitian degeneracies in a

chaotic exciton-polariton billiard, Nature (London) **526**, 554 (2015).
[39] Y. Wu, W. Liu, J. Geng, X. Song, X. Ye, C.-K. Duan, X. Rong, and J. Du, Observation of parity-time symmetry breaking in a single-spin system, Science **364**, 878 (2019).
[40] W. Zhang, X. Ouyang, X. Huang, X. Wang, H. Zhang, Y. Yu, X. Chang, Y. Liu, D.-L. Deng, and L.-M. Duan, Observation of non-Hermitian topology with nonunitary dynamics of solid-state spins, Phys. Rev. Lett. **127**, 090501 (2021).
[41] M. Naghiloo, M. Abbasi, Y. N. Joglekar, and K. Murch, Quantum state tomography across the exceptional point in a single dissipative qubit, Nat. Phys. **15**, 1232 (2019).
[42] W. Heiss and H. Harney, The chirality of exceptional points, Eur. Phys. J. D **17**, 149 (2001).
[43] M. Berry, Physics of nonHermitian degeneracies, Czech. J. Phys. **54**, 1039 (2004).
[44] C. Dembowski, B. Dietz, H.-D. Gräf, H. L. Harney, A. Heine, W. D. Heiss, and A. Richter, Encircling an exceptional point, Phys. Rev. E **69**, 056216 (2004).
[45] W. Heiss, The physics of exceptional points, J. Phys. A: Math. Theor. **45**, 444016 (2012).
[46] H. Jing, Ş. Özdemir, H. Lü, and F. Nori, High-order exceptional points in optomechanics, Sci. Rep. **7**, 1 (2017).
[47] C. M. Bender and S. Boettcher, Real spectra in non-Hermitian hamiltonians having $\mathscr{P}\mathscr{T}$ symmetry, Phys. Rev. Lett. **80**, 5243 (1998). C. M. Bender, Making sense of non-Hermitian hamiltonians, Rep. Prog. Phys. **70**, 947 (2007).
[48] T. Fukui and N. Kawakami, Breakdown of the Mott insulator: Exact solution of an asymmetric Hubbard model, Phys. Rev. B **58**, 16051 (1998).
[49] T. Oka and H. Aoki, Dielectric breakdown in a Mott insulator: Many-body Schwinger-Landau-Zener mechanism studied with a generalized bethe ansatz, Phys. Rev. B **81**, 033103 (2010).
[50] T. E. Lee and C.-K. Chan, Heralded magnetism in non-Hermitian atomic systems, Phys. Rev. X **4**, 041001 (2014).
[51] T. E. Lee, F. Reiter, and N. Moiseyev, Entanglement and spin squeezing in non-Hermitian phase transitions, Phys. Rev. Lett. **113**, 250401 (2014).
[52] Y. Ashida, S. Furukawa, and M. Ueda, Parity-time-symmetric quantum critical phenomena, Nat. Commun. **8**, 15791 (2017).
[53] R. Couvreur, J. L. Jacobsen, and H. Saleur, Entanglement in nonunitary quantum critical spin chains, Phys. Rev. Lett. **119**, 040601 (2017).
[54] M. Nakagawa, N. Kawakami, and M. Ueda, Non-Hermitian kondo effect in ultracold alkaline-earth atoms, Phys. Rev. Lett. **121**, 203001 (2018).
[55] L. Herviou, J. H. Bardarson, and N. Regnault, Defining a bulk-edge correspondence for non-Hermitian Hamiltonians via singular-value decomposition, Phys. Rev. A **99**, 052118 (2019); L. Herviou, N. Regnault, and J. H. Bardarson, Entanglement spectrum and symmetries in non-Hermitian fermionic non-interacting models, SciPost Phys. **7**, 069 (2019).
[56] K. Yamamoto, M. Nakagawa, K. Adachi, K. Takasan, M. Ueda, and N. Kawakami, Theory of non-Hermitian fermionic superfluidity with a complex-valued interaction, Phys. Rev. Lett. **123**, 123601 (2019).
[57] P.-Y. Chang, J.-S. You, X. Wen, and S. Ryu, Entanglement spectrum and entropy in topological non-Hermitian systems and nonunitary conformal field theory, Phys. Rev. Res. **2**, 033069 (2020).
[58] Y.-T. Tu, Y.-C. Tzeng, and P.-Y. Chang, Rényi entropies and negative central charges in non-Hermitian quantum systems, SciPost Phys. **12**, 194 (2022).
[59] C. H. Lee, Exceptional bound states and negative entanglement entropy, Phys. Rev. Lett. **128**, 010402 (2022).
[60] K. Kawabata, T. Numasawa, and S. Ryu, Entanglement phase transition induced by the non-Hermitian skin effect, Phys. Rev. X **13**, 021007 (2023).
[61] T. E. Lee, Anomalous edge state in a non-Hermitian lattice, Phys. Rev. Lett. **116**, 133903 (2016).
[62] S. Yao and Z. Wang, Edge states and topological invariants of non-Hermitian systems, Phys. Rev. Lett. **121**, 086803 (2018).
[63] S. Yao, F. Song, and Z. Wang, Non-Hermitian chern bands, Phys. Rev. Lett. **121**, 136802 (2018).
[64] F. K. Kunst, E. Edvardsson, J. C. Budich, and E. J. Bergholtz, Biorthogonal bulk-boundary correspondence in non-Hermitian systems, Phys. Rev. Lett. **121**, 026808 (2018).
[65] M. S. Rudner and L. S. Levitov, Topological transition in a non-Hermitian quantum walk, Phys. Rev. Lett. **102**, 065703 (2009).
[66] K. Esaki, M. Sato, K. Hasebe, and M. Kohmoto, Edge states and topological phases in non-Hermitian systems, Phys. Rev. B **84**, 205128 (2011).
[67] Y. C. Hu and T. L. Hughes, Absence of topological insulator phases in non-Hermitian PT-symmetric hamiltonians, Phys. Rev. B **84**, 153101 (2011).
[68] H. Schomerus, Topologically protected midgap states in complex photonic lattices, Opt. Lett. **38**, 1912 (2013).
[69] S. Longhi, D. Gatti, and G. D. Valle, Robust light transport in non-Hermitian photonic lattices, Sci. Rep. **5**, 13376 (2015).
[70] D. Leykam, K. Y. Bliokh, C. Huang, Y. D. Chong, and F. Nori, Edge modes, degeneracies, and topological numbers in non-Hermitian systems, Phys. Rev. Lett. **118**, 040401 (2017).
[71] Y. Xu, S.-T. Wang, and L.-M. Duan, Weyl exceptional rings in a three-dimensional dissipative cold atomic gas, Phys. Rev. Lett. **118**, 045701 (2017).
[72] H. Shen, B. Zhen, and L. Fu, Topological band theory for non-Hermitian Hamiltonians, Phys. Rev. Lett. **120**, 146402 (2018).
[73] Z. Gong, Y. Ashida, K. Kawabata, K. Takasan, S. Higashikawa, and M. Ueda, Topological phases of non-Hermitian systems, Phys. Rev. X **8**, 031079 (2018).
[74] K. Kawabata, S. Higashikawa, Z. Gong, Y. Ashida, and M. Ueda, Topological unification of time-reversal and particle-hole symmetries in non-Hermitian physics, Nat. Commun. **10**, 297 (2019).
[75] K. Kawabata, K. Shiozaki, M. Ueda, and M. Sato, Symmetry and topology in non-Hermitian physics, Phys. Rev. X **9**, 041015 (2019).
[76] H. Zhou and J. Y. Lee, Periodic table for topological bands with non-Hermitian symmetries, Phys. Rev. B **99**, 235112 (2019).
[77] H.-G. Zirnstein, G. Refael, and B. Rosenow, Bulk-boundary correspondence for non-Hermitian Hamiltonians via green functions, Phys. Rev. Lett. **126**, 216407 (2021).
[78] D. S. Borgnia, A. J. Kruchkov, and R.-J. Slager, Non-Hermitian boundary modes and topology, Phys. Rev. Lett. **124**, 056802 (2020).

[79] K. Kawabata, T. Bessho, and M. Sato, Classification of exceptional points and non-Hermitian topological semimetals, Phys. Rev. Lett. **123**, 066405 (2019).
[80] J. Y. Lee, J. Ahn, H. Zhou, and A. Vishwanath, Topological correspondence between Hermitian and non-Hermitian systems: Anomalous dynamics, Phys. Rev. Lett. **123**, 206404 (2019).
[81] K. Kawabata, K. Shiozaki, and S. Ryu, Topological field theory of non-Hermitian systems, Phys. Rev. Lett. **126**, 216405 (2021).
[82] Y. Xiong, Why does bulk boundary correspondence fail in some non-Hermitian topological models, J. Phys. Commun. **2**, 035043 (2018).
[83] V. M. Martinez Alvarez, J. E. Barrios Vargas, and L. E. F. Foa Torres, Non-Hermitian robust edge states in one dimension: Anomalous localization and eigenspace condensation at exceptional points, Phys. Rev. B **97**, 121401(R) (2018).
[84] A. McDonald, T. Pereg-Barnea, and A. A. Clerk, Phase-dependent chiral transport and effective non-Hermitian dynamics in a bosonic Kitaev-Majorana chain, Phys. Rev. X **8**, 041031 (2018).
[85] C. H. Lee and R. Thomale, Anatomy of skin modes and topology in non-Hermitian systems, Phys. Rev. B **99**, 201103(R) (2019).
[86] T. Liu, Y.-R. Zhang, Q. Ai, Z. Gong, K. Kawabata, M. Ueda, and F. Nori, Second-order topological phases in non-Hermitian systems, Phys. Rev. Lett. **122**, 076801 (2019).
[87] C. H. Lee, L. Li, and J. Gong, Hybrid higher-order skin-topological modes in nonreciprocal systems, Phys. Rev. Lett. **123**, 016805 (2019).
[88] K. Yokomizo and S. Murakami, Non-bloch band theory of non-Hermitian systems, Phys. Rev. Lett. **123**, 066404 (2019).
[89] N. Okuma and M. Sato, Quantum anomaly, non-Hermitian skin effects, and entanglement entropy in open systems, Phys. Rev. B **103**, 085428 (2021).
[90] K. Zhang, Z. Yang, and C. Fang, Correspondence between winding numbers and skin modes in non-Hermitian systems, Phys. Rev. Lett. **125**, 126402 (2020).
[91] N. Okuma, K. Kawabata, K. Shiozaki, and M. Sato, Topological origin of non-Hermitian skin effects, Phys. Rev. Lett. **124**, 086801 (2020).
[92] Y. Li, C. Liang, C. Wang, C. Lu, and Y.-C. Liu, Gain-loss-induced hybrid skin-topological effect, Phys. Rev. Lett. **128**, 223903 (2022).
[93] F. Song, S. Yao, and Z. Wang, Non-Hermitian skin effect and chiral damping in open quantum systems, Phys. Rev. Lett. **123**, 170401 (2019).
[94] T. Haga, M. Nakagawa, R. Hamazaki, and M. Ueda, Liouvillian skin effect: Slowing down of relaxation processes without gap closing, Phys. Rev. Lett. **127**, 070402 (2021).
[95] C.-H. Liu, K. Zhang, Z. Yang, and S. Chen, Helical damping and dynamical critical skin effect in open quantum systems, Phys. Rev. Res. **2**, 043167 (2020).
[96] T. Mori and T. Shirai, Resolving a discrepancy between liouvillian gap and relaxation time in boundary-dissipated quantum many-body systems, Phys. Rev. Lett. **125**, 230604 (2020).
[97] F. Yang, Q.-D. Jiang, and E. J. Bergholtz, Liouvillian skin effect in an exactly solvable model, Phys. Rev. Res. **4**, 023160 (2022).
[98] W.-T. Xue, M.-R. Li, Y.-M. Hu, F. Song, and Z. Wang, Simple formulas of directional amplification from non-bloch band theory, Phys. Rev. B **103**, L241408 (2021).
[99] P. Wen, M. Wang, and G.-L. Long, Optomechanically induced transparency and directional amplification in a non-Hermitian optomechanical lattice, Opt. Express **30**, 41012 (2022).
[100] S. Longhi, Self-healing of non-Hermitian topological skin modes, Phys. Rev. Lett. **128**, 157601 (2022).
[101] K. Zhang, C. Fang, and Z. Yang, Dynamical degeneracy splitting and directional invisibility in non-Hermitian systems, Phys. Rev. Lett. **131**, 036402 (2023).
[102] K. Zhang, Z. Yang, and C. Fang, Universal non-Hermitian skin effect in two and higher dimensions, Nat. Commun. **13**, 2496 (2022).
[103] L. Mao, T. Deng, and P. Zhang, Boundary condition independence of non-Hermitian Hamiltonian dynamics, Phys. Rev. B **104**, 125435 (2021).
[104] W.-T. Xue, Y.-M. Hu, F. Song, and Z. Wang, Non-Hermitian edge burst, Phys. Rev. Lett. **128**, 120401 (2022).
[105] S. E. Skipetrov and I. M. Sokolov, Absence of Anderson localization of light in a random ensemble of point scatterers, Phys. Rev. Lett. **112**, 023905 (2014).
[106] S. Skipetrov and I. Sokolov, Magnetic-field-driven localization of light in a cold-atom gas, Phys. Rev. Lett. **114**, 053902 (2015).
[107] C. E. Máximo, N. Piovella, P. W. Courteille, R. Kaiser, and R. Bachelard, Spatial and temporal localization of light in two dimensions, Phys. Rev. A **92**, 062702 (2015).
[108] L. Lo, P. T. Fong, and C. K. Law, Dynamical Casimir effect in resonance fluorescence, Phys. Rev. A **102**, 033703 (2020).
[109] L. Bellando, A. Gero, E. Akkermans, and R. Kaiser, Cooperative effects and disorder: A scaling analysis of the spectrum of the effective atomic Hamiltonian, Phys. Rev. A **90**, 063822 (2014).
[110] G. L. Celardo and L. Kaplan, Superradiance transition in one-dimensional nanostructures: An effective non-Hermitian Hamiltonian formalism, Phys. Rev. B **79**, 155108 (2009).
[111] E. Akkermans, A. Gero, and R. Kaiser, Photon localization and Dicke superradiance in atomic gases, Phys. Rev. Lett. **101**, 103602 (2008).
[112] W. Guerin, M. O. Araújo, and R. Kaiser, Subradiance in a large cloud of cold atoms, Phys. Rev. Lett. **116**, 083601 (2016).
[113] N. Goldman, J. C. Budich, and P. Zoller, Topological quantum matter with ultracold gases in optical lattices, Nat. Phys. **12**, 639 (2016).
[114] A. Cresti, Convenient peierls phase choice for periodic atomistic systems under magnetic field, Phys. Rev. B **103**, 045402 (2021).
[115] Y. Yi and Z. Yang, Non-Hermitian skin modes induced by on-site dissipations and chiral tunneling effect, Phys. Rev. Lett. **125**, 186802 (2020).
[116] C.-H. Liu and S. Chen, Information constraint in open quantum systems, Phys. Rev. B **104**, 174305 (2021).
[117] L. Wang, Q. Liu, and Y. Zhang, Quantum dynamics on a lossy non-Hermitian lattice*, Chin. Phys. B **30**, 020506 (2021).
[118] P. Wen, J. Pi, and G.-L. Long, Investigation of a non-Hermitian edge burst with time-dependent perturbation theory, Phys. Rev. A **109**, 022236 (2024).

[119] Q.-B. Zeng, Non-Hermitian skin effect edge, Phys. Rev. B **106**, 235411 (2022).

[120] C. Yuce and H. Ramezani, Non-Hermitian edge burst without skin localization, Phys. Rev. B **107**, L140302 (2023).

[121] Y.-M. Hu, W.-T. Xue, F. Song, and Z. Wang, Steady-state edge burst: From free-particle systems to interaction-induced phenomena, Phys. Rev. B **108**, 235422 (2023).

[122] Z. Cai and T. Barthel, Algebraic versus exponential decoherence in dissipative many-particle systems, Phys. Rev. Lett. **111**, 150403 (2013).

[123] L. Xiao, T. Deng, K. Wang, Z. Wang, W. Yi, and P. Xue, Observation of non-bloch parity-time symmetry and exceptional points, Phys. Rev. Lett. **126**, 230402 (2021).

[124] W. Gou, T. Chen, D. Xie, T. Xiao, T.-S. Deng, B. Gadway, W. Yi, and B. Yan, Tunable nonreciprocal quantum transport through a dissipative Aharonov-Bohm ring in ultracold atoms, Phys. Rev. Lett. **124**, 070402 (2020).

[125] J. Wen, C. Zheng, Z. Ye, T. Xin, and G. Long, Stable states with nonzero entropy under broken $\mathcal{PT}$ symmetry, Phys. Rev. Res. **3**, 013256 (2021).